Stochastic nanoroughness modulates neuron–astrocyte interactions and function via mechanosensing cation channels

Nils R. Blumenthal[a,b], Ola Hermanson[c], Bernd Heimrich[d], and V. Prasad Shastri[a,b,1]

[a]Institute for Macromolecular Chemistry, [b]BIOSS Centre for Biological Signalling Studies, and [d]Department of Neuroanatomy, University of Freiburg, 79104 Freiburg, Germany; and [c]Department of Neuroscience, Karolinska Institutet, SE17177 Stockholm, Sweden

Edited* by Robert Langer, Massachusetts Institute of Technology, Cambridge, MA, and approved October 8, 2014 (received for review July 8, 2014)

Extracellular soluble signals are known to play a critical role in maintaining neuronal function and homeostasis in the CNS. However, the CNS is also composed of extracellular matrix macromolecules and glia support cells, and the contribution of the physical attributes of these components in maintenance and regulation of neuronal function is not well understood. Because these components possess well-defined topography, we theorize a role for topography in neuronal development and we demonstrate that survival and function of hippocampal neurons and differentiation of telencephalic neural stem cells is modulated by nanoroughness. At roughnesses corresponding to that of healthy astrocytes, hippocampal neurons dissociated and survived independent from astrocytes and showed superior functional traits (increased polarity and calcium flux). Furthermore, telencephalic neural stem cells differentiated into neurons even under exogenous signals that favor astrocytic differentiation. The decoupling of neurons from astrocytes seemed to be triggered by changes to astrocyte apical-surface topography in response to nanoroughness. Blocking signaling through mechanosensing cation channels using GsMTx4 negated the ability of neurons to sense the nanoroughness and promoted decoupling of neurons from astrocytes, thus providing direct evidence for the role of nanotopography in neuron–astrocyte interactions. We extrapolate the role of topography to neurodegenerative conditions and show that regions of amyloid plaque buildup in brain tissue of Alzheimer's patients are accompanied by detrimental changes in tissue roughness. These findings suggest a role for astrocyte and ECM-induced topographical changes in neuronal pathologies and provide new insights for developing therapeutic targets and engineering of neural biomaterials.

mechanotransduction | stretch-activated channels | FAM38A | Piezo-1 | polarization

Cellular homeostasis in the brain tissue is believed to be regulated primarily by a complex spatiotemporal signaling environment involving soluble neurotrophic factors (1, 2). These factors, including neurotrophins such as brain-derived neurotrophic factor, the TGF-β family including bone morphogenetic proteins (BMPs), and the IL-6 superfamily including ciliary neurotrophic factor (CNTF), regulate survival, steer progenitor fate decision, and critically affect the development of the nervous system as well as the homeostasis of the adult CNS (3–6). However, developmental processes such as axon pathfinding, synapse formation, nervous system patterning, neuronal plasticity, and degeneration fail to be explained solely on the basis of soluble factors. There is increasing evidence that physical variables such as the stiffness of a cellular environment influence cell development (7–12). However, the cells of the brain tissue reside in a soft environment that is rich in polysaccharides (13, 14). In the context of neuronal development and neurophysiology, astrocytes have an established role in maintaining neuronal function. They form a vast network that provides the physical and biochemical matrix over which neurons thrive and function (15, 16). The plasticity found in the brain can be attributed in part to the morphological changes that occur in astrocyte processes that can not only alter the geometry of the neuronal environment but also induce dynamic changes in astrocyte–neuron interactions affecting neurotransmission, signal gradients, and the relationship between synapses (15). Interestingly, the changes to the physical aspects of a neuronal environment can originate from changes to morphology of support cells such as astrocytes and also changes to ECM structure and properties. Cells and ECM polysaccharides play an important role in growth, differentiation, and migration of neural precursors, as well as in repair and plasticity in the central nervous system (17, 18). However, in addition to a biological function, cells and macromolecules provide a physically defined environment (19, 20), and we postulate a significant role for topography in neural development. Studies to date have focused on the effects of microscale topography, deterministic roughness, and substrate chemistry on neurite outgrowth and neuronal function (7, 21–23). However, the influence of ECM-like nanotopography on neuronal development and fate is a realm that has not been investigated thus far. Therefore, in this work we specifically focus on the impact of stochastic nanoroughness as would be provided by neighboring cells and ECM molecules on neuronal cell interactions, function, and differentiation.

Significance

The role of soluble signals in neural differentiation and neurodegeneration is well established. However, the impact of nanotopography imposed by macromolecules within brain tissue on neuronal function and pathologies is not fully appreciated. We have discovered that nanoroughness can modulate the function of hippocampal neurons and their relationship with astrocytes. Inhibition of mechanosensing cation channels including Piezo-1, whose distribution is altered by nanotopography, abrogates the effects imposed by nanotopography and the association of neurons with astrocytes. The finding that regions of amyloid plaque buildup in Alzheimer's involve changes to tissue nanoroughness provides a link between nanoscale physical cues and loss of function in neurons and may have implications in uncovering the factors that promote neurodegenerative diseases.

Author contributions: N.R.B. and V.P.S. designed research; N.R.B. performed research; O.H. and B.H. contributed new reagents/analytic tools; O.H. provided scientific input and laboratory facilities to carry out the studies involving telencephalic neural stem cells and designed siRNA sequence for FAM38 silencing studies; B.H. provided scientific input and laboratory facilities to isolate hippocampal neurons; N.R.B., B.H., and V.P.S. analyzed data; and N.R.B., O.H., B.H., and V.P.S. wrote the paper.

The authors declare no conflict of interest.

*This Direct Submission article had a prearranged editor.

[1]To whom correspondence should be addressed. Email: prasad.shastri@gmail.com.

This article contains supporting information online at www.pnas.org/lookup/suppl/doi:10.1073/pnas.1412740111/-/DCSupplemental.

Results and Discussion

Nanotopography Modulates PC-12 Cell Polarity and Enhances Function. Because macromolecules are in a state of high entropy, and entropy is a statistical measure of randomness, the roughness presented by macromolecules is expected to be stochastic (random). We simulated random ECM nanoroughness using an assembly of monodispersed silica colloids of increasing size (10, 24) (Fig. 1*A*). The roughness in this system scales logarithmically with nanoparticle radius and can recapitulate topography from the level of receptor clusters to ECM features (25) and further allows the production of surfaces with stochastic nanoroughness (surface kurtosis ≤3, Table S1). In contrast, surfaces consisting of periodic grooves and ridges that have been extensively studied present deterministic roughness. As a first step we investigated the ability of PC-12 cells (26), a well-established model system for studying neuronal differentiation, to perceive stochastic nanoroughness and analyzed changes to their morphology and function. PC-12 cells are indeed able to perceive the underlying nanoroughness but in an NGF- and collagen-dependent manner (Fig. S1) and, more importantly, showed an increased differentiation and associated functional traits on a specific R_q of ∼32 nm as evident from a highly polarized cell morphology (Fig. 1*B*, *Middle*) and associated changes such as fewer and longer neurite outgrowths (Fig. 1 *C* and *D*) compared with glass, which is considered a smooth substrate (R_q ∼3.5 nm, Fig. 1*B*, *Left*). Beyond this optimal substrate roughness cells were more prone to clumping (Fig. 1*B*, *Right*). Such a loss in neuronal polarity and clumping has also been observed by Brunetti et al. (7) in SH-SY5Y cells grown on gold surfaces with high prescribed nanoroughness. One measure of the functional state of a neuron is the activity of acetylcholinesterase (AChE), because this is necessary for synaptic communication. Interestingly, AChE levels also peaked in PC-12 cells on 32-nm R_q surfaces (Fig. 1*E*), which also coincided with an accelerated and elevated calcium response to depolarization (Fig. 1 *F* and *G*).

Nanotopography Mediates Hippocampal Neuron–Astrocyte Interaction. We then posed the following question: Can neuronal cells in general perceive nanoroughness, and if so does it have a role in defining their interaction and function? Hippocampal neurons are responsible for memory formation. Loss of their function and death has been linked to neuropathologies such as Alzheimer's. We therefore evaluated the response of mixed primary cultures of rat hippocampal neurons and astrocytes to the different roughness regimes. Surprisingly, primary hippocampal neurons also responded to roughness in a manner similar to dopaminergic PC-12 and exhibited prominent, axon-like polarized structures on exactly the same R_q of 32 nm (Fig. S2). A more remarkable finding was that nanoroughness seemed to modulate the relationship and dependency of neurons on astrocytes. It is well established that neurons require astrocytes for survival (27) and, indeed, on surfaces with an R_q above and below 32 nm

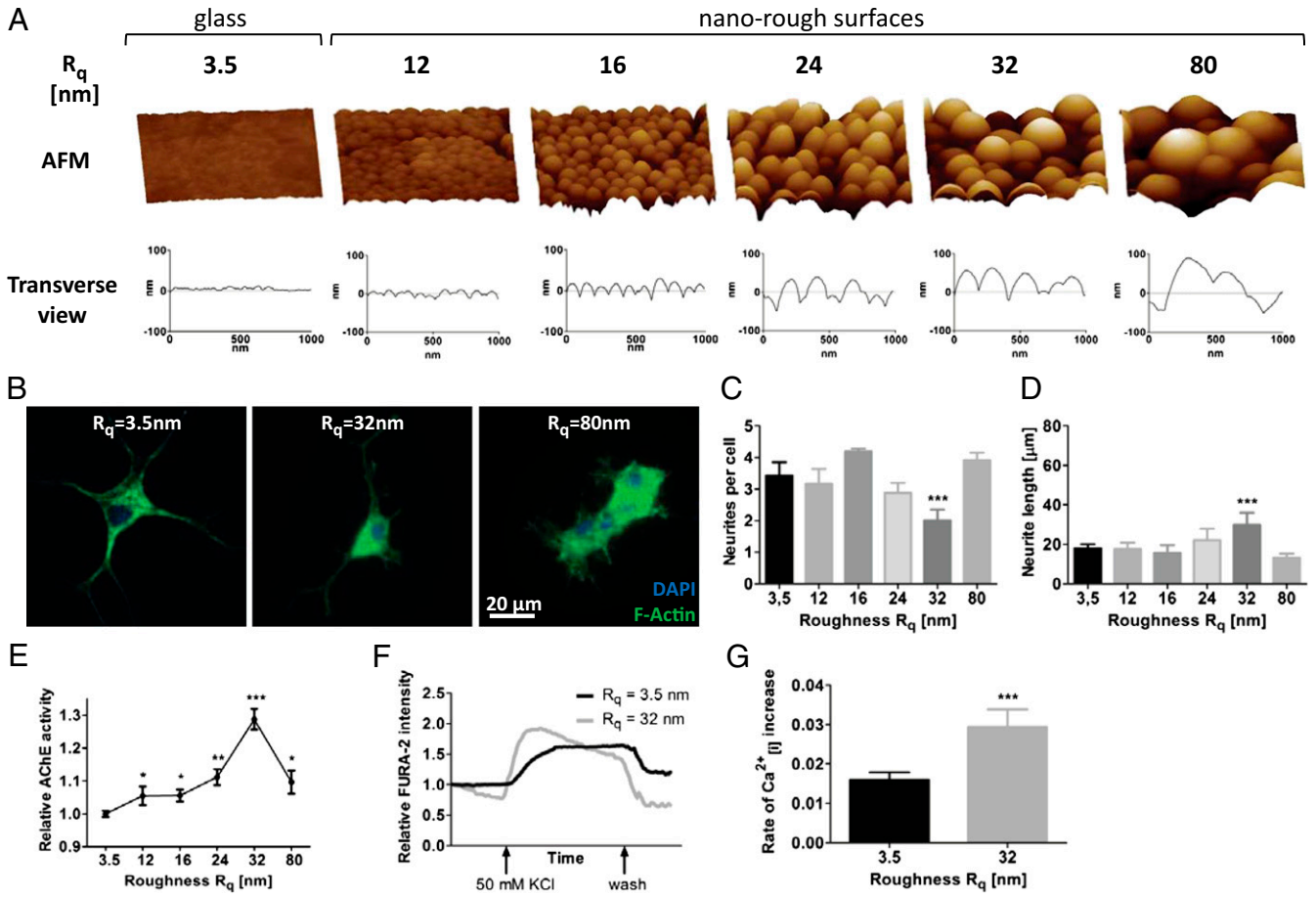

Fig. 1. Morphological and functional traits in PC-12 cells on nanorough substrates. (*A*) AFM of SNP modified substrates with the corresponding surface roughness R_q. (*B*) Morphology of PC-12 cells on R_q = 3.5 nm, R_q = 32 nm, and R_q = 80 nm visualized by staining for F-actin. Impact of nanoroughness on PC-12 polarization as assessed by determining (*C*) number of neurites per cell and (*D*) neurite length. (*E*) Influence of nanoroughness on AChE activity. Calcium-sensitive FURA-2 imaging of differentiated PC-12 cells on smooth glass substrates and surfaces with an R_q of 32 nm: (*F*) change in intracellular calcium levels as assessed by FURA-2 intensity and (*G*) rate of depolarization as determined by the slope of the depolarization portion of the curve (immediately after addition of KCl). Statistical significance: $*P < 0.05$; $**P < 0.01$; $***P < 0.001$.

neurons were predominantly found associated with astrocytes (Fig. 2 *A* and *C*). However, on R_q of ∼32 nm neurons were dissociated from astrocytes (Fig. 2 *B* and *C*) and continued to survive independently even up to 6 wk (Fig. 2*D*). After 5 d, the percentage of neurons that were associated with astrocytes on the 32-nm R_q surface was around 15%, which was 1.5- to twofold lower than those on other R_qs, which ranged from 20–40%, and sixfold lower than that on the smooth glass substrate (Fig. 2*C*). That is, in comparison with the other R_qs, over twice as many neurons on the 32-nm R_q surface were surviving independently of astrocytes. Because the isolation procedure yields a mixture of hippocampal neurons and astrocytes, differences in cell density might be a contributing factor. Analysis of the astrocyte and neuron density at day 5 showed no significant differences in density and population distribution between glass and 32-nm R_q surfaces, indicating that the observed effects cannot be attributed to cell density and population variations (Fig. S3). At 6 wk, however, the percentage of neurons that were surviving independently of astrocytes on the 32-nm R_q was over sixfold greater in comparison with the other R_qs. Whereas over 90% of neurons were associated with astrocytes on other roughnesses, only 15% of neurons were associated with astrocytes on the 32-nm R_q (Fig. 2*D*). Remarkably, hippocampal neurons on 32-nm R_q surfaces, despite being dissociated from astrocytes, showed an order of magnitude faster and stronger increase in intracellular calcium levels following membrane depolarization in comparison with those on smooth surfaces (Fig. 2 *E* and *F*). So, there seemed to be a favorable R_q of around 32 nm at which both PC-12 and hippocampal neurons seemed to be more functional.

Mechanosensing Ion Channels Including Piezo-1 Are Responsible for the Sensing of Nanoscale Physical Cues by Neurons. Past studies showed that stochastic nanoroughness altered the organization of focal adhesion complexes in highly migratory preosteoblasts and endothelial cells (24). Because neurons have limited migratory capacity (28), a critical open question was how neurons perceive nanoroughness. Scanning electron micrographs revealed that the neurites indeed make intimate contact with the underlying topography (Fig. 3*A*). Such intimate contact between the neurites and the surface ought to manifest itself as changes in membrane tension. Because the conformation and distribution of mechanosensitive ion channels are altered in response to changes in membrane tension and curvature (29–31), we probed the expression pattern of FAM38A, an integrin-activated transmembrane protein that is part of the mechanosensitive ion channel Piezo-1 (32). Piezo-1 is expressed by CNS neurons and not by sensory neurons such as dorsal root ganglia (DRGs) (33). It was observed that whereas FAM38A expression in PC-12 cells on glass was predominantly localized at neurite branch points, which would be a region of high cytoskeletal tension (Fig. 3*B*), in contrast a more uniform distribution of FAM38A could be seen on the optimal R_q of 32 nm, suggesting a dramatic change to the mechanical environment of the neurites as they perceive the nanoroughness (Fig. 3*C*). Because FAM38A expression level was not altered (Fig. S4), and PC-12 during differentiation did not show any changes in attachment force (Fig. S5) or motility (Fig. S6) in response to nanoroughness, the observed changes to the Piezo-1 expression pattern can be linked to the underlying nanotopography. In contrast to CNS neurons, DRGs do not express Piezo-1 but express other stretch-activated cation channels (SACs) such as Piezo-2, TRPC1, and TRCP6. Interestingly, DRGs do not show any morphological changes on nanoroughness substrates (Fig. 3 *D* and *E*), and nanotopography has no effect on calcium influx and depolarization patterns (Fig. 3 *F* and *G*). Therefore, this suggests a prominent role for Piezo-1 in sensing nanotopography.

Neuron–Astrocyte Interactions Involve Topographical Cues Provided by Astrocytes and SACs. As indicated earlier, primary hippocampal neurons require interaction with astrocytes for their survival (27). This raised the question of why the neurons favor the

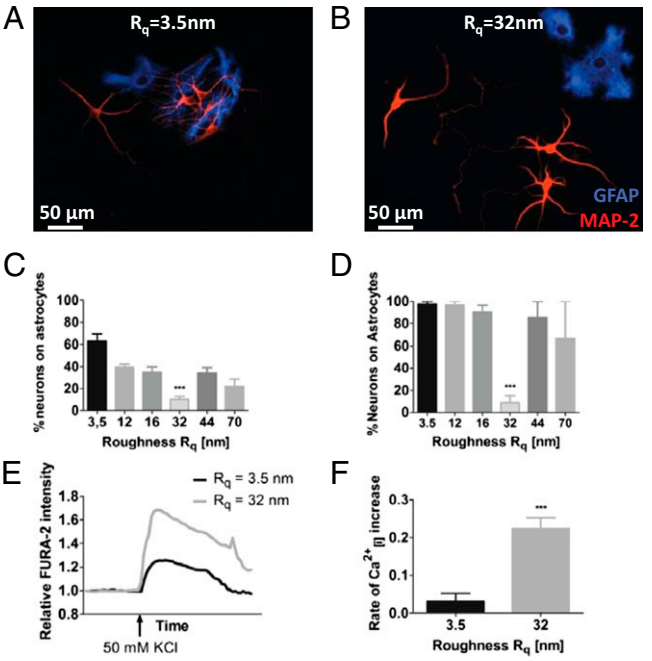

Fig. 2. Morphology and function of rat hippocampal neurons and astrocytes are influenced by substrate roughnesses. Neuron–astrocyte interaction on (*A*) smooth glass substrate and (*B*) substrate of R_q = 32 nm. Astrocytes were visualized using antibody against GFAP (blue) and neurons were visualized using antibody against MAP-2 (red). Quantification of neuron–astrocyte association in (*C*) short-term cultures (5 d) and (*D*) long-term cultures (6 wk). Calcium-sensitive FURA-2 imaging in hippocampal neurons on smooth glass substrates and surfaces with R_q of 32 nm: (*E*) change in intracellular calcium level as assessed by FURA-2 intensity and (*F*) rate of depolarization as determined by the slope of the depolarization portion of the curve (immediately after addition of KCl). Statistical significance: ***$P < 0.001$.

surface over association with the astrocytes. Atomic force microscopy (AFM) analysis of the surface of astrocytes associated with neurons led us to the remarkable finding that the roughness of the astrocyte surface was around an R_q of 26–28 nm (see Fig. 5*D*) and this coincides rather well with the roughness regime on which neurons exhibit decoupling from astrocytes. A role of mechanotransduction in maintaining neuron–astrocyte interactions is further supported by our findings that inhibition of signaling through SACs (Piezo-1, TRPC1, and TRPC 6) using GsMTx4, a peptide extracted from spider venom (34, 35), promotes decoupling of neurons from astrocytes even on smooth glass substrates (Fig. 3 *H* and *I*) where they normally show strong association (Fig. 2 *A*, *C*, and *D*). Furthermore, the increased sensitivity to depolarization that was observed in hippocampal neurons on R_q of 32 nm is lost upon inhibition of SACs (Fig. 3 *J* and *K*). To specifically delineate the role of Piezo-1, an siRNA knockdown of FAM38 RNA expression was undertaken in hippocampal neuron/astrocyte mixed cultures, because astrocytes and hippocampal neurons cannot be easily separated. Surprisingly, Piezo-1 knockdown at >60% mRNA levels was lethal to astrocytes but not to neurons (Fig. S7). Death of astrocytes could be attributed to Piezo-1 knockdown and not to toxicity owing to transfection agent or siRNA, because nontarget siRNA and transfection agent alone were not lethal to astrocytes. This provides direct evidence for the role of nanotopography in influencing hippocampal neuron–astrocyte interaction and function through mechanotransduction via SACs.

Telencephalic Neural Stem-Cell Differentiation to Neurons Is Enhanced at Roughness Corresponding to That of Healthy Astrocytes. Because stochastic nanoroughness can replicate the physical cues presented by astrocytes, we explored whether topography can influence

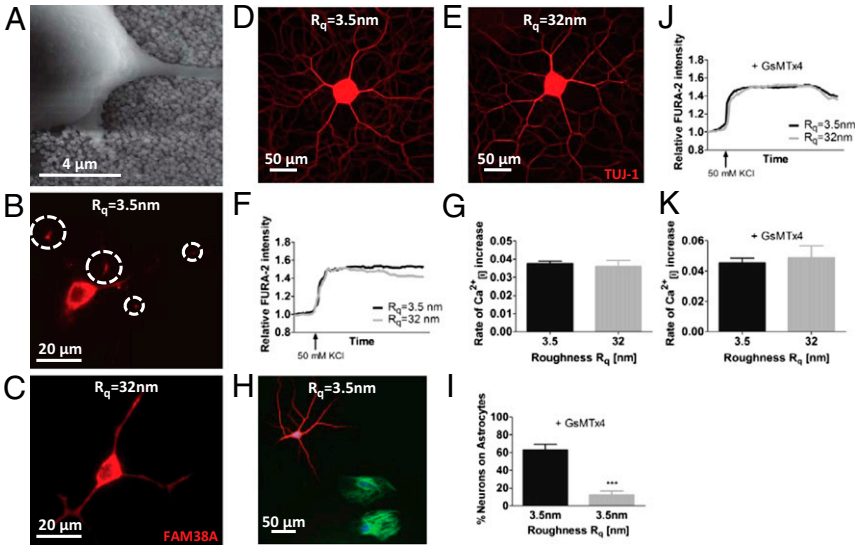

Fig. 3. Piezo-1 is necessary for sensing nanotopography. (*A*) Representative scanning electron micrograph of PC-12 cells grown on nanorough surface (shown $R_q = 40$ nm). PC-12 stained using anti-FAM38A, an antibody for Piezo-1 mechanosensitive ion channel on $R_q = 3.5$ nm (*B*) and $R_q = 32$ nm (*C*). On smooth surfaces, FAM38A staining is pronounced at neurite branch points (denoted by circles) (*B*), whereas on nanorough surfaces FAM38A staining is uniform along all neurite processes (*C*). Rat dorsal root ganglia morphology (*D* and *E*) and function (*F* and *G*) on glass and R_q of 32 nm. Inhibition of FAM38A with GsMTx4 (5 μM) results in decoupling of hippocampal neurons from astrocytes on smooth glass substrates (*H* and *I*). The FURA-2 intensity profile (*J*) and rate of calcium influx (*K*) in hippocampal neurons upon depolarization with KCl on smooth glass substrate and $R_q = 32$ nm is identical upon inhibition of FAM38A. Statistical significance: ***$P < 0.001$.

neural progenitor cell differentiation and lineage commitment as well. To answer this we followed the spontaneous and soluble signal-induced lineage commitment of telencephalic neural stems cells (NSCs) from embryonic rats (embryonic day 15.5) (36) on various R_q regimes. These NSCs remain undifferentiated in the presence of FGF2, whereas withdrawal of this factor leads to spontaneous differentiation where a majority of the cells become astrocytes (37, 38). After 7 d in culture, on the preferred R_q of 32 nm and additionally on an R_q of 16 nm, a 10- to 20-fold greater number of NSCs showed spontaneous differentiation to neurons, as assessed by positive staining for MAP-2, a marker for postmitotic neurons (Fig. 4 *A* and *B*). However, more remarkably, even upon exposure to CNTF, which under this condition is known to promote differentiation of NSCs to astrocytes, after 2 d a twofold increase in NSCs positive for the neuron-specific class III β-tubulin (TuJ1 antibody), an early marker for commitment to neuronal phenotype, was observed on the R_qs of 32 nm and 16 nm (Fig. 4 *C* and *D*). The stimulus provided by CNTF, therefore, seemed to compete with that provided by the nanoroughness. The localization of MAP-2 primarily occurred around the nucleus like a cap, with nascent neurite outgrowths also staining positive for MAP-2. This is consistent with the process of maturation of neuronal progenitors into neurons. However, exposure to BMP4/Wnt3a, which increases the efficiency of neuronal differentiation of NSCs (36), resulted in no qualitative differences between NSCs on the various R_qs and glass and tissue culture polystyrene (TCPS) controls (Fig. S8). These results suggest an essential modulatory role for nanoroughness in combination with soluble signals. Interestingly, once again there seemed to be a favored regime of R_q (16–32 nm), bounded by roughnesses that did not favor neuronal differentiation.

Nanoroughness Alters Apical Roughness of Healthy Astrocytes. It is becoming evident that astrocytes, in addition to providing soluble survival factors to neurons, may also be critical in providing physical cues that are necessary for neuron function and survival. The decoupling of the hippocampal neurons from the astrocytes on surfaces with R_q of 32 nm can be linked to fundamental changes that take place in the astrocytes on these surfaces. We observed that on R_q of 32 nm, in addition to assuming a more migratory phenotype (Fig. S9), which was confirmed by a decrease in the astrocyte form factor (Fig. 5*A*), the roughness of the astrocyte surface is significantly increased from an R_q 26–30 nm on smooth surfaces (Fig. 5 *B* and *D*) to an R_q of 68–72 nm on a 32-nm rough surface (Fig. 5 *C* and *D*). This finding provides a direct link between the physical properties of the cell surface and underlying substrate roughness. Because we observed that R_qs greater than 60 nm promoted neuronal cell death, one might suggest that the decoupling of the neuron–astrocyte interaction on 32-nm R_q may be a driven by the unfavorable changes to the physical environment provided by the astrocytes, thus implying that healthy astrocytes have both a neuroprotective (i.e., they secrete neurotrophic factors) and a more critical structural support role that is necessary for neuronal survival and differentiation. This conclusion is also consistent with our current observation that inhibition mechanosensing eliminates association of neurons and astrocytes, and an earlier observation that astrocytes possess different surface topographies depending on whether they are permissive or nonpermissive to neuronal growth (39). These observations in sum suggest a role for nanotopography in modulating the membrane tension in neurites,

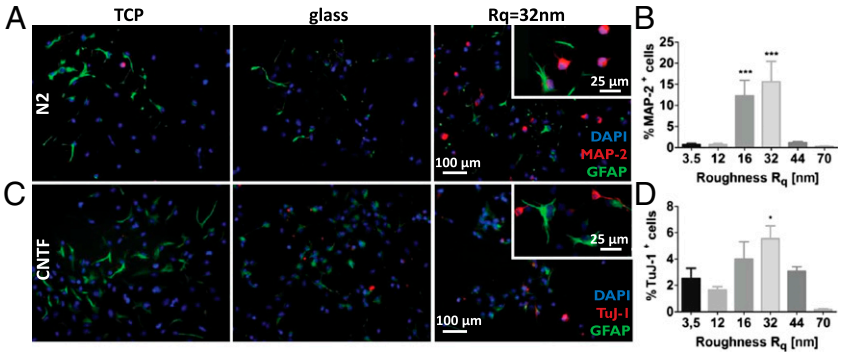

Fig. 4. Nanoroughness mediates rat telencephalic NSC lineage commitment and differentiation. NSC differentiation on TCPS glass, and substrates with R_q of 32 nm. (*A*) Spontaneous differentiation in N2 media in absence of any exogenous soluble signals (blue, DAPI nuclear stain; red, MAP-2; green, GFAP astrocyte marker), (*B*) quantification of Map-2^+ NSC in the absence of growth factors, (*C*) differentiation in the presence of CNTF (blue, DAPI nuclear stain; red, Tuj-1; green, GFAP astrocyte marker), and (*D*) quantification of Tuj-1^+ NSC when exposed to CNTF. Statistical significance: *$P < 0.05$; ***$P < 0.001$.

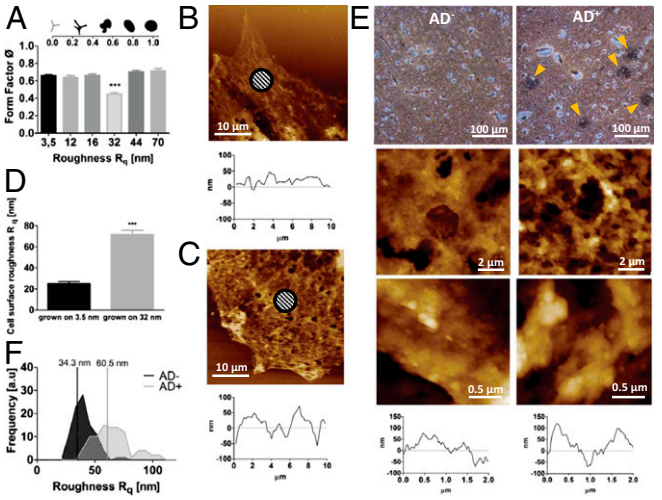

Fig. 5. Nanoroughness alters physical attributes of astrocytes. Dependence of astrocyte form factor on substrate nanoroughness. (*A*) Decrease in form factor on 32-nm R_q surfaces is consistent with a more motile phenotype (*Inset*). Morphological changes to astrocyte cell surface on nanorough surfaces: AFM images of astrocytes grown on glass (*B*) and on R_q = 32 nm (*C*) and the corresponding transverse line scans and changes to topography of astrocyte surface on 32-nm surfaces (*D*). Shaded areas show representative areas for R_q calculations. Amyloid-β plaques are associated with topographical changes to brain tissue. Paraffin-embedded human brain slices stained with Bielschowsky's silver stain (*E*). (*Left*) Healthy human (AD^-). (*Right*) Patient diagnosed with Alzheimer's (AD^+) revealing amyloid-β plaques indicated by yellow arrowheads. (*Middle and Bottom*) Tapping mode AFM scans (10 × 10 μm) of one of the representative areas above, higher-magnification (2 × 2 μm) scan of the same area, and transverse views of the corresponding 2- × 2-μm image above. (*F*) Histograms of R_q values of healthy brain tissue and amyloid-β plaques in Alzheimer's patients showing a general shift of tissue roughness to higher R_qs and an increased heterogeneity in roughness in AD^+ brain slices. R_q values were calculated using a 700- × 700-nm scan area.

which in turn can lead to alterations in intracellular signaling pathways and a change in the functional state of the neuron.

Regions of Amyloid Plaque Buildup in Alzheimer's Present Increased Tissue Nanoroughness. Our observation that the topography of astrocytes, support cells for neurons, can dictate the function of the phenotypically unrelated neurons points to a larger paradigm wherein physical and mechanical information provided by astrocytes and ECM macromolecules play a role not only in neuronal development but also in neuropathologies. There is ample evidence that the loss of memory associated with Alzheimer's disease (AD) is due to the death of hippocampal neurons. Chondroitin sulfate proteoglycans (CSPGs) have been implicated both in neural differentiation and neuropathologies such as Alzheimer's (17). CSPGs have been found to colocalize with amyloid-β plaques, and in vitro studies have shown that CSPGs can promote amyloid-β fibril assembly, a key step in plaque formation. Interestingly, amyloid-β stimulates CSPG production in astrocytes, which has negative effects on neuronal health and synapse formation. This is consistent with reports that neuronal differentiation is inhibited when neurons are exposed to amyloid-β (40). It has been demonstrated that changes to CSPG structure through sulfation can alter its function and role in neural differentiation (18). We have recently shown that the secondary structure of polysaccharides can be dramatically altered through a simple oxidative modification of the backbone, and this is accompanied by changes to nanotopography and macromolecular organization (41). It is thus plausible that changes to the functional role of CSPGs upon sulfation or other oxidative chemistries are a result of changes to their secondary structures and topography. This prompted us to theorize that the loss of hippocampal neuron function in Alzheimer's may be triggered by changes to the topography that the neurons experience.

To investigate this premise further, we analyzed the topographical characteristics of amyloid-β plaques in the hippocampus of human brain slices using AFM (Fig. 5*E*). We made a compelling observation that whereas the R_q of healthy brain tissue (AD^-) showed a Gaussian distribution with a median centered around 34 nm, the tissue of individuals diagnosed with Alzheimer's (AD^+) showed a bimodal distribution of tissue roughness with a pronounced shift in the median toward higher R_q values of 60 nm accompanied by a more heterogeneous R_q pattern (Fig. 5*F*). The emergence of R_q values greater than 80 nm, which is the range of R_q where we observe increased neuronal cell death, is in accordance with published reports that neurons when exposed to amyloid-β undergo apoptosis (40, 42). Our earlier findings that cell shape can be affected by nanoroughness (10) and our current observation that astrocyte shape is affected by nanoroughness provide evidence that cell signaling in the neuronal environment may be additionally mediated by ECM-based cues.

The effects of stochastic nanoroughness on neuronal health can manifest itself in two possible scenarios: (*i*) The changes to tissue roughness affect glial cell behavior, which then instigates changes to the neuron signaling environment, and/or (*ii*) the changes to the tissue roughness alter the way neurons and glial cells perceive their physical environment. Dynamic changes to astrocyte–neuron interaction mediated by changes to distal astrocytic processes are known to influence neuron–astrocyte plasticity (15). Although astrocytes are generally stationary cells that provide a supportive network for neuronal cells and synapses, migratory and proliferating astrocytes have been observed in glial scarring, an environment with diminished neuronal function (43, 44). In this study, an altered cellular environment in the form of nanotopography was shown to affect astrocyte biophysical attributes (shape and roughness) so as to alter their interaction with neurons. However, strong evidence for the second scenario is derived from a recent study by Satoh et al. (45) that showed that hMib (a synonym for Piezo-1) is transcriptionally induced in activated astrocytes associated with senile amyloid-β plaques in AD^+ human brains. Interestingly, neurons that express hMib show damaged morphology whereas healthy-looking neurons do not express hMib. The ability to sense the changes to astrocyte topography induced by tissue roughness may have triggered undesirable changes in $hMib^+$ neurons. Conversely, the inability to sense the mechanical cues provided by the astrocytes may play a role in the loss of function in the $hMib^-$ neurons. Because healthy neurons are $hMib^+$, loss of this marker may additionally play a role in the functional deficiency associated with Alzheimer's. In sum, the key findings of this study provide evidence for the hitherto unexplored role for ECM and glial cell-associated changes to stochastic nanoroughness in neurodevelopment and neuropathologies. These new insights should prove valuable in the development of new therapeutic targets and design principles for engineering materials and interfaces for neural interfacing.

Materials and Methods

Substrate Preparation. Silica (SiO_2) nanoparticles were synthesized by the Stöber process as described earlier (46). By changing the amount of ammonia, water, and tetraethylorthosilicate (TEOS; Sigma) in the reaction the particle diameter could be controlled. Successful silica nanoparticle (SNP) synthesis was confirmed by dynamic light scattering with the particle analyzer DelsaNano C equipped with the DelsaNano Software V3.73/2.3 (Beckman Coulter Inc.). Following spin-coating of the particles onto clean glass slides and a drying period of 12 h at 200 °C substrates were characterized by AFM (as described later) to ensure the correct surface roughness. For cell culture experiments, SNP modified substrates from eight independent nanoparticle preparations were used at least in duplicate.

SEM. See *SI Materials and Methods*.

AFM. See *SI Materials and Methods*.

Cell Culture. All animal procedures were approved by the animal welfare committees of the State of Baden Württemberg and the University of Freiburg

(Regierungspräsidium Freiburg Az: 35/9185.81/X-11/05S) and by Stockholms Norra Djurförsöksetiskanämnd (ethical permit N284/11). PC-12 cells were obtained from the American Type Culture Collection (CRL-1721) and cultured in suspension in RPMI media supplemented with 10% (vol/vol) horse serum and 5% (vol/vol) FBS in a humidified incubator at 37 °C. Differentiation was induced by seeding cells onto collagen IV-coated substrates in media supplemented with 1% horse serum and 100 ng/mL NGF (R&D Systems). For primary hippocampus cultures, newborn Wistar rats (postnatal days 1–3) were killed by decapitation. The hippocampi were isolated followed by a trypsin digestion and mechanical dissociation. If not stated differently, cells were seeded as 7.5×10^4 cells/cm^2. After 12 h media was changed for serum-free neurobasal media supplemented with B27 and glutamine and further cultured for 5 d in a humidified incubator at 37 °C and 8% CO_2 before analysis. For dorsal root ganglia cell culture, Wistar rats (postnatal days 10–15) were killed by CO_2 intoxication following isoflurane anesthesia. Spines were removed and cleaned of connective tissue and muscles. After opening the spines along the acanthi and opposite along the vertebral bodies, dorsal root ganglia were isolated, freed of nerve fibers, and collected in ice-cold PBS. To obtain a single-cell suspension, ganglia were incubated in collagenase (end concentration 20 μg/mL) and trypsin for 20 min at 37 °C followed by mechanical dissociation and several washing steps. For cell culture, 5×10^4 cells/cm^2 were seeded in α-MEM media containing 15% FBS, 1% penicillin/streptomycin, and 5 ng/mL NGF and cultures were maintained in a humidified incubator at 37 °C and 5% CO_2. For telencephalic stem cells, timed pregnant Wistar rats (embryonic day 15.5) were killed by CO_2 intoxication. Embryos were removed and the cortices isolated and collected in Hank's solution. Following mechanical dissociation, cells were seeded onto polylysine-coated Petri dishes in N2 media supplemented with 10 ng/mL FGF2. Media was changes daily until the culture was 90% confluent. For differentiation experiments, cells were detached with Hank's solution and 10^5 cells were seeded onto the respective polylysine-coated substrates in N2 media containing 10 ng/mL FGF2. The following day, media was changed to N2 media containing CNTF (10 ng/mL), BMP4 + Wnt3 (both 10 ng/mL), or no growth factors. Differentiation cultures were maintained for 48 h (CNTF differentiation) or 7 d (BMP4 + Wnt3 and spontaneous differentiation) before analysis.

Piezo-1 Inhibition Studies. The stretch-activated ion channel Piezo-1 was inhibited with the peptidyl toxin GsMTx4 (5 μM) isolated from the *Grammostola rosea* tarantula venom.

Immunocytochemistry. For a discussion of morphological analysis, calcium-sensitive imaging, acetylcholinesterase activity measurement, and immunohistochemistry of AD slices see *SI Materials and Methods*.

ACKNOWLEDGMENTS. The authors thank Ms. S. Zenker (University of Freiburg) for assistance with rat hippocampal neuron isolation and staining protocols, Dr. Michalina Lewicka (Karolinska Institutet) for help in isolating neural stem cells, the Life Imaging Center and Prof. R. Nitschke (University of Freiburg) for assistance with calcium-sensitive imaging, Dr. R. Thomann (University of Freiburg) for SEM pictures, and Prof. Marco Prinz and Dr. Ori Staszewski (Institute for Neuropathology, University of Freiburg) for providing us with human brain slices. This work was funded by the Excellence Initiative of the German Federal and State Governments Grant EXC 294.

1. Álvarez-Palazuelos LE, et al. (2011) Regulation of neural stem cell in the human SVZ by trophic and morphogenic factors. *Curr Signal Transduct Ther* 6(3):320–326.
2. Steindler DA, Pincus DW (2002) Stem cells and neuropoiesis in the adult human brain. *Lancet* 359(9311):1047–1054.
3. Dessaud E, et al. (2007) Interpretation of the sonic hedgehog morphogen gradient by a temporal adaptation mechanism. *Nature* 450(7170):717–720.
4. Deverman BE, Patterson PH (2009) Cytokines and CNS development. *Neuron* 64(1):61–78.
5. Rowitch DH, Kriegstein AR (2010) Developmental genetics of vertebrate glial-cell specification. *Nature* 468(7321):214–222.
6. Steventon B, Araya C, Linker C, Kuriyama S, Mayor R (2009) Differential requirements of BMP and Wnt signalling during gastrulation and neurulation define two steps in neural crest induction. *Development* 136(5):771–779.
7. Brunetti V, et al. (2010) Neurons sense nanoscale roughness with nanometer sensitivity. *Proc Natl Acad Sci USA* 107(14):6264–6269.
8. Engler AJ, Sen S, Sweeney HL, Discher DE (2006) Matrix elasticity directs stem cell lineage specification. *Cell* 126(4):677–689.
9. Ferrari A, et al. (2011) Nanotopographic control of neuronal polarity. *Nano Lett* 11(2): 505–511.
10. Lipski AM, Pino CJ, Haselton FR, Chen I-W, Shastri VP (2008) The effect of silica nanoparticle-modified surfaces on cell morphology, cytoskeletal organization and function. *Biomaterials* 29(28):3836–3846.
11. Mammoto A, Mammoto T, Ingber DE (2012) Mechanosensitive mechanisms in transcriptional regulation. *J Cell Sci* 125(Pt 13):3061–3073.
12. Teixeira AI, et al. (2009) The promotion of neuronal maturation on soft substrates. *Biomaterials* 30(27):4567–4572.
13. Brizzi MF, Tarone G, Defilippi P (2012) Extracellular matrix, integrins, and growth factors as tailors of the stem cell niche. *Curr Opin Cell Biol* 24(5):645–651.
14. Ellison K, Zwolinski C (2011) Neural stem cell response to endothelial-derived extracellular matrix produced by hemodynamically stimulated endothelial cells. *Proceedings of the 2011 IEEE 37th Annual Northeast Bioengineering Conference* (IEEE, New York), pp 19–20.
15. Theodosis DT, Poulain DA, Oliet SH (2008) Activity-dependent structural and functional plasticity of astrocyte-neuron interactions. *Physiol Rev* 88(3):983–1008.
16. Wade JJ, McDaid LJ, Harkin J, Crunelli V, Kelso JA (2011) Bidirectional coupling between astrocytes and neurons mediates learning and dynamic coordination in the brain: A multiple modeling approach. *PLoS ONE* 6(12):e29445.
17. Galtrey CM, Fawcett JW (2007) The role of chondroitin sulfate proteoglycans in regeneration and plasticity in the central nervous system. *Brain Res Brain Res Rev* 54(1):1–18.
18. Gu W-L, et al. (2009) Chondroitin sulfate proteoglycans regulate the growth, differentiation and migration of multipotent neural precursor cells through the integrin signaling pathway. *BMC Neurosci* 10:128.
19. Raspanti M, Alessandrini A, Ottani V, Ruggeri A (1997) Direct visualization of collagen-bound proteoglycans by tapping-mode atomic force microscopy. *J Struct Biol* 119(2):118–122.
20. Ng L, et al. (2003) Individual cartilage aggrecan macromolecules and their constituent glycosaminoglycans visualized via atomic force microscopy. *J Struct Biol* 143(3):242–257.
21. Lovat V, et al. (2005) Carbon nanotube substrates boost neuronal electrical signaling. *Nano Lett* 5(6):1107–1110.
22. Schmidt CE, Shastri VR, Vacanti JP, Langer R (1997) Stimulation of neurite outgrowth using an electrically conducting polymer. *Proc Natl Acad Sci USA* 94(17):8948–8953.
23. Song M, Uhrich KE (2007) Optimal micropattern dimensions enhance neurite outgrowth rates, lengths, and orientations. *Ann Biomed Eng* 35(10):1812–1820.
24. Lipski M, et al. (2007) Nanoscale engineering of biomaterial surfaces. *Adv Mater* 19(4):553–557.
25. Shastri VP (2009) In vivo engineering of tissues: Biological considerations, challenges, strategies, and future directions. *Adv Mater* 21(32–33):3246–3254.
26. Greene LA, Tischler AS (1976) Establishment of a noradrenergic clonal line of rat adrenal pheochromocytoma cells which respond to nerve growth factor. *Proc Natl Acad Sci USA* 73(7):2424–2428.
27. Cui W, Allen ND, Skynner M, Gusterson B, Clark AJ (2001) Inducible ablation of astrocytes shows that these cells are required for neuronal survival in the adult brain. *Glia* 34(4):272–282.
28. Fricker RA, et al. (1999) Site-specific migration and neuronal differentiation of human neural progenitor cells after transplantation in the adult rat brain. *J Neurosci* 19(14):5990–6005.
29. Nilius B (2010) Pressing and squeezing with Piezos. *EMBO Rep* 11(12):902–903.
30. Charras GT, Williams BA, Sims SM, Horton MA (2004) Estimating the sensitivity of mechanosensitive ion channels to membrane strain and tension. *Biophys J* 87(4): 2870–2884.
31. Martinac B (2004) Mechanosensitive ion channels: Molecules of mechanotransduction. *J Cell Sci* 117(Pt 12):2449–2460.
32. Coste B, et al. (2010) Piezo1 and Piezo2 are essential components of distinct mechanically activated cation channels. *Science* 330(6000):55–60.
33. Roudaut Y, et al. (2012) Touch sense: Functional organization and molecular determinants of mechanosensitive receptors. *Channels (Austin)* 6(4):234–245.
34. Delmas P, Hao J, Rodat-Despoix L (2011) Molecular mechanisms of mechanotransduction in mammalian sensory neurons. *Nat Rev Neurosci* 12(3):139–153.
35. Bae C, Sachs F, Gottlieb PA (2011) The mechanosensitive ion channel Piezo1 is inhibited by the peptide GsMTx4. *Biochemistry* 50(29):6295–6300.
36. Andersson T, et al. (2011) Noggin and Wnt3a enable BMP4-dependent differentiation of telencephalic stem cells into GluR-agonist responsive neurons. *Mol Cell Neurosci* 47(1):10–18.
37. Hermanson O, Jepsen K, Rosenfeld MG (2002) N-CoR controls differentiation of neural stem cells into astrocytes. *Nature* 419(6910):934–939.
38. Johe KK, Hazel TG, Muller T, Dugich-Djordjevic MM, McKay RD (1996) Single factors direct the differentiation of stem cells from the fetal and adult central nervous system. *Genes Dev* 10(24):3129–3140.
39. Weissmüller G, Garcia-Abreu J, Mascarello Bisch P, Moura Neto V, Cavalcante LA (2000) Glial cells with differential neurite growth-modulating properties probed by atomic force microscopy. *Neurosci Res* 38(2):217–220.
40. Fraser PE, Lévesque L, McLachlan DR (1994) Alzheimer A beta amyloid forms an inhibitory neuronal substrate. *J Neurochem* 62(3):1227–1230.
41. Forget A, et al. (2013) Polysaccharide hydrogels with tunable stiffness and provasculogenic properties via α-helix to β-sheet switch in secondary structure. *Proc Natl Acad Sci USA* 110(32):12887–12892.
42. Ivins KJ, Thornton PL, Rohn TT, Cotman CW (1999) Neuronal apoptosis induced by beta-amyloid is mediated by caspase-8. *Neurobiol Dis* 6(5):440–449.
43. Buffo A, Rolando C, Ceruti S (2010) Astrocytes in the damaged brain: molecular and cellular insights into their reactive response and healing potential. *Biochem Pharmacol* 79(2):77–89.
44. Wanner IB, et al. (2013) Glial scar borders are formed by newly proliferated, elongated astrocytes that interact to corral inflammatory and fibrotic cells via STAT3-dependent mechanisms after spinal cord injury. *J Neurosci* 33(31):12870–12886.
45. Satoh K, et al. (2006) A novel membrane protein, encoded by the gene covering KIAA0233, is transcriptionally induced in senile plaque-associated astrocytes. *Brain Res* 1108(1):19–27.
46. Stöber W, Fink A, Bohn E (1968) Controlled growth of monodisperse silica spheres in the micron size range. *J Colloid Interface Sci* 26(1):62–69.